Dartmouth College
Dartmouth Digital Commons

Open Dartmouth: Faculty Open Access Articles

1-2010

A New Technique for Firn Grain-Size Measurement Using Sem Image Analysis

N.E. Spaulding
University of Maine

D.A. Meese
Dartmouth College

I. Baker
Dartmouth College

P.A. Mayewski
University of Maine

Follow this and additional works at: https://digitalcommons.dartmouth.edu/facoa

Part of the Glaciology Commons

Recommended Citation

Instruments and Methods

A new technique for firn grain-size measurement using SEM image analysis

N.E. SPAULDING,[1] D.A. MEESE,[1,2] I. BAKER,[2] P.A. MAYEWSKI,[1] G.S. HAMILTON[1]

[1]Climate Change Institute, University of Maine, 303 Bryand Global Sciences Center, Orono, Maine 04469-5790, USA
E-mail: nicole.spaulding@maine.edu
[2]Thayer School of Engineering, Dartmouth College, Hanover, New Hampshire 03755-8000, USA

ABSTRACT. Firn microstructure is accurately characterized using images obtained from scanning electron microscopy (SEM). Visibly etched grain boundaries within images are used to create a skeleton outline of the microstructure. A pixel-counting utility is applied to the outline to determine grain area. Firn grain sizes calculated using the technique described here are compared to those calculated using the techniques of Gow (1969) and Gay and Weiss (1999) on samples of the same material, and are found to be substantially smaller. The differences in grain size between the techniques are attributed to sampling deficiencies (e.g. the inclusion of pore filler in the grain area) in earlier methods. The new technique offers the advantages of greater accuracy and the ability to determine individual components of the microstructure (grain and pore), which have important applications in ice-core analyses. The new method is validated by calculating activation energies of grain boundary diffusion using predicted values based on the ratio of grain-size measurements between the new and existing techniques. The resulting activation energy falls within the range of values previously reported for firn/ice.
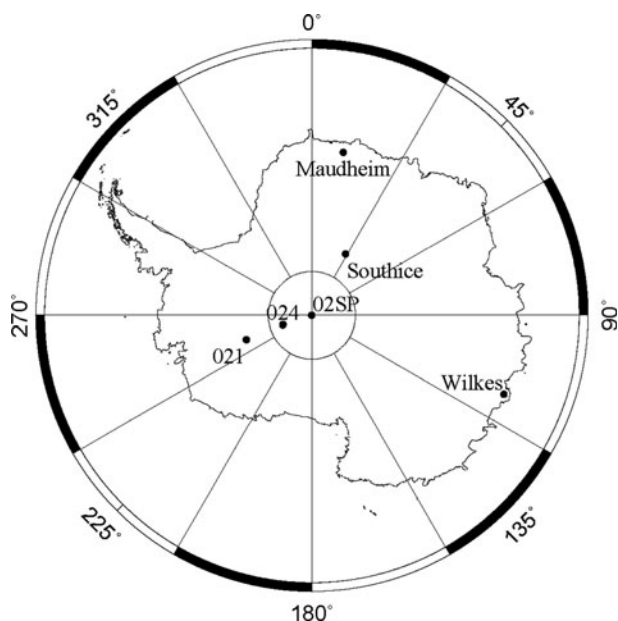
INTRODUCTION

Firn and ice cores, such as those collected by the International Trans-Antarctic Scientific Expedition (ITASE) (Mayewski and Goodwin, 1997; Mayewski and others, 2005), contain information about the soluble, insoluble and gaseous components of the atmosphere, as well as indicators of temperature, precipitation, atmospheric circulation, sea-ice extent and volcanic activity (Legrand and Mayewski, 1997). Microstructural parameters, including grain size and porosity, provide additional information about atmospheric temperature changes, impurity content, accumulation rate and deformation history. Therefore, accurate measurements of grain size and porosity allow for the identification of layers that do not exhibit normal grain growth with depth, and the detection of anomalous changes in any of the factors affecting the growth and sintering of firn and ice grains, i.e. impurity concentration, grain boundary pinning, stress and strain conditions, recrystallization, annealing, deformation and recovery. Spatial variations in microstructure provide insights into micrometeorological conditions such as snow accumulation and wind patterns (Rick and Albert, 2004) that potentially affect the preservation of paleoclimate records. In addition, the microstructure of near-surface firn influences the reflection of electromagnetic radiation, thereby affecting remote-sensing and radar studies (e.g. Zwally and others, 1977; Surdyk, 2002).

Despite the importance of firn microstructure to paleo-climate reconstructions, little progress has been made in the measurement of firn grain size. The original method of grain-size measurement (Gow, 1969) used the average of the shortest and longest axes of the 50 largest grains as measured with a pocket comparator (a hand-held magnification tool for making linear measurements). Alley (1980) modified this method slightly by excluding the five largest grains in the sample. Subsequent methods evolved to counting all grains

within a known area (Duval and Lorius, 1980) or using the linear intercept method which expresses grain size as an average length by counting the number of grain boundary intersections along a known length (e.g. Thorsteinsson and others, 1995; Alley and Woods, 1996). A newer method uses digital images of thin sections, and automated outlining and pixel-counting software to derive grain size as a mean cross-sectional area (Gay and Weiss, 1999). These techniques, which were developed to measure grains of all sizes, have seen only limited use in the study of firn because of the difficulty involved in processing firn samples.

The differences between the above techniques represent attempts to resolve the two primary sources of uncertainty in the estimation of grain size: how to calculate and report 'size', and how to account for the cut effect and the intersection probability effect (Higgins, 2000). Both uncertainties arise from measuring an irregular three-dimensional structure using a two-dimensional image. The first source is a matter of determining which parameter (length or area) is most closely related to grain volume. The latter source results from the act of sectioning. When a thin section is created, it is unknown at which point and in how many places each grain has been cut. The plane from which average grain size is calculated will include cross-sections ranging from small grain tips to the maximum grain diameter. Thus a range of sizes will be found even for a homogeneously sized population: the so-called cut effect. An additional source of uncertainty arises because smaller crystals are less likely to be intersected by the plane: the intersection probability effect (Higgins, 2000).

Each of the techniques discussed above has unique problems as well as common disadvantages. Traditional methods of grain-size measurement in firn (e.g. Gow, 1969; Duval and Lorius, 1980; Alley and Woods, 1996; Gay and Weiss, 1999) require the use of a pore filler (e.g. aniline or

Fig. 1. Map of core sites. Ice cores 02-1, 02-4 and 02-SP were used in this study to calculate grain sizes and growth rates. Maudheim, Southice, Wilkes and two locations not shown (Site 2, Greenland, and South Pole) were used in Figure 4.

METHODS

There is considerable confusion surrounding the definitions of crystals and grains. Gow (1969) defines a grain as a unit having up to three crystals. The crystals within a grain are distinguished by changes in birefringence under crossed polarizers. In materials science, polycrystalline materials are made up of individual grains each of which is a single crystal. These variations in terminology have caused confusion between fields. The term grain, as used here, is in line with the materials science definition. We use this definition because visibly etched boundaries which typically align with a change in axis orientation (Baker and others, 2005; Obbard and others, 2006; Sieg, 2008) can be seen clearly in SEM images.

Grain-size measurements from three firn and ice cores (02-1, 02-4 and 02-SP) collected during the 2002 US ITASE traverse in East Antarctica (Fig. 1) were derived using the techniques of Gow (1969), Gay and Weiss (1999) and the new technique described below. Samples were taken at those depths from which high-quality digital thin-section photographs existed, and enough sample remained to prepare an SEM specimen. Several cores were used in order to span the range of depths desired. For the first two techniques, thin-section samples were photographed under crossed polarizers with both a film camera and a digital camera (Fig. 2). The photographs were used to calculate grain size (Gow and others, 2004) using the methods of Gow (1969). These data are referred to as 'GOW'. The digital images were analyzed using the Image Pro Plus 5.0® software package which automatically outlines grains (as differentiated by birefringence patterns; Fig. 2b) and counts the pixels within each grain (Gay and Weiss, 1999). These samples are referred to as 'G&W'.

Our new technique entails the examination of SEM specimens using a Field Emission Gun (FEI) XL30 SEM operated at 15 kV with a beam current of 0.15 nA. Samples were maintained at $-110 \pm 5°C$ using a custom-designed liquid nitrogen chilled cold stage (Baker and others, 2007). For each sample, a series of slightly overlapping secondary electron images was collected and digitally stitched together to form a mosaic of the horizontal surface of the sample (Fig. 3a). Grain sizes were determined by manually tracing grain boundaries using Image Pro Plus 5.0® to create a
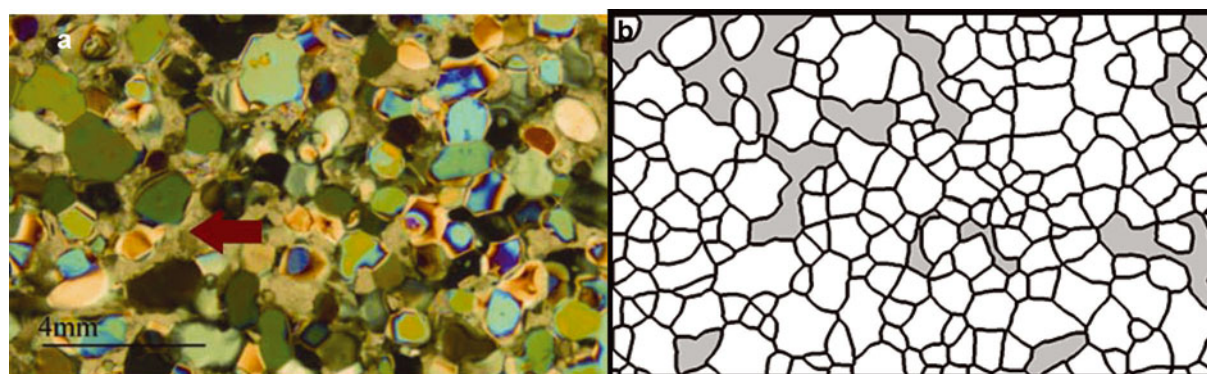
dodecane) because of the fragile nature of firn. The pore filler, despite its utility, obscures details of the microstructure, making accurate measurements difficult. This problem can be mitigated by using scanning electron microscopy (SEM). The SEM imaging technique of Baker and others (2007) provides high-resolution images of both grain and pore structure with minimal sample preparation. Because it requires no pore filler, SEM analysis allows visualization of both grain and pore geometry. This imaging technique is used in combination with a new measurement technique, described in this paper, to eliminate most of the uncertainties of past measurement techniques. A comparison between grain-size measurements, growth rates and apparent activation energies calculated using this method and earlier methods reveals a number of differences. Our analysis of these differences has implications for paleoclimate reconstructions using ice cores.

Fig. 2. (a) Thin section 02-1 16m under crossed polarizers. Red arrow points to pore filler used in the preparation of thin sections, which obscures the microstructure. (b) Skeleton outline of grains. Gray portions indicate areas where pore filler has overlapped grains enough to obscure their shape. Outlines are thickened for visibility at this scale. The two large grains to the left and immediately above the red arrow illustrate the 'cut effect'. These grains appear larger than all the others and all the grains in Figure 3 because they were likely intersected at their widest point.
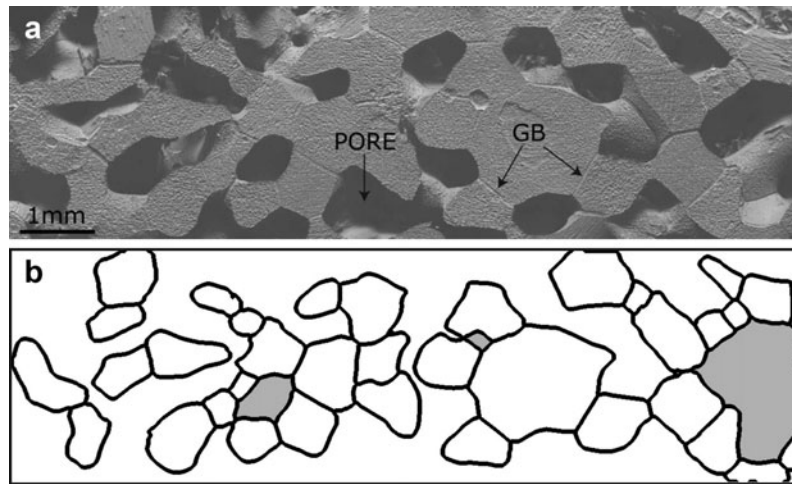
Fig. 3. (a) SEM image of 02-1 16m. SEM images require no pore filler, so most aspects of the microstructure are clearly visible. Prominent features such as pores and clearly etched grain boundaries (GB) which aid in the identification of individual grains are labeled. (b) The skeleton outline of grain boundaries. Pores that are fully bound by grains are colored gray. Boundary thickness is amplified for ease of visibility.

skeleton outline of the boundaries (Fig. 3b). A pixel-counting utility was applied to the skeleton outline to determine the grain area. These samples are referred to as 'SPLD'.

We adopt the practice of reporting mean grain size as a cross-sectional area based on all grains in the section, for several reasons. A computer simulation of normal grain growth by Anderson and others (1989) indicates that using the mean cross-sectional area of all grains in the section is the combination of parameters most likely to eliminate the uncertainties of the cut effect and the intersection probability effect. In their model, grains greater in size than the average grain size (as derived using all grains in the section) grew, whereas those smaller than the average grain size shrank. These model results indicate that mean grain size obtained using all grains in the section has a particular physical significance, which is not the case for only the largest grains. Anderson and others (1989) also noted the similarity of grain growth kinetics derived from mean grain volume to those based on mean grain cross-sectional area when grain morphology was consistently compact and the surface-area to volume ratio was minimal.

RESULTS AND DISCUSSION
Grain size

Grain size is a function of both age/depth and temperature (Stephenson, 1967; Gow, 1969). The linear relationship between age and mean grain cross-section is:

$$\overline{A} = \overline{A}_0 + Kt,$$

where $\overline{A}$ is the measured mean cross-sectional area (mm^2) at time t, $\overline{A}_0$ is the extrapolated mean cross-sectional area at $t = 0$, and K is the rate of grain growth. The equation rests on the assumption that growth rate is controlled by interfacial tension at the grain boundaries (Cole and others, 1954). The temperature dependence of K is described by the Arrhenius-type equation

$$K = K_0 \exp\left(-\frac{E_a}{RT}\right),$$

where T is temperature in kelvin, K_0 is an empirical constant and E_a and R are the activation energy of grain boundary self-diffusion and the gas constant respectively. E_a is determined by the slope of the temperature grain growth (T–K) curve. This type of dependence is appropriate because the ratio of the activation energy of grain boundary self-diffusion to volume self-diffusion (determined experimentally) for ice ($\sim$6 : 10) is similar to that for most metals (Gow and others, 2004).

Grain sizes calculated using the three different techniques described above are plotted against depth for each core in Figure 4. As expected, grain size increases with depth. Correlation coefficients were computed between grain size and depth for each method. The highest correlation between size and depth was for GOW samples (0.86), followed by SPLD (0.66) and G&W (0.48), indicating that site-to-site variations in grain size are masked by including only the 50 largest grains. There are additional reasons for the differences in correlation, as discussed below.
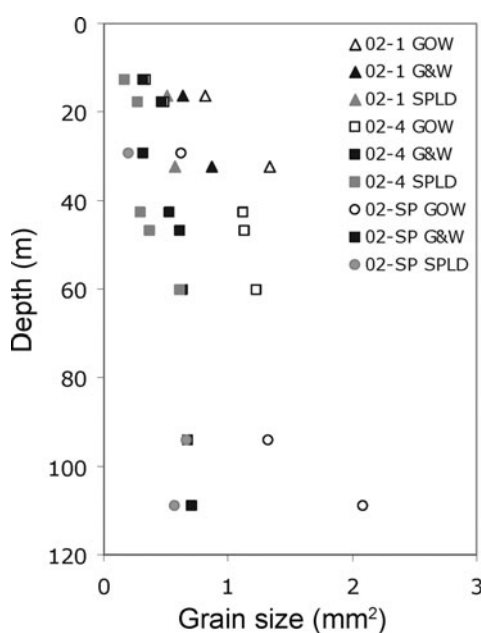
Fig. 4. Grain size versus depth using three different measurement techniques. GOW average 57.1% larger than SPLD; G&W average 27.8% larger than SPLD. Data from Table 1.
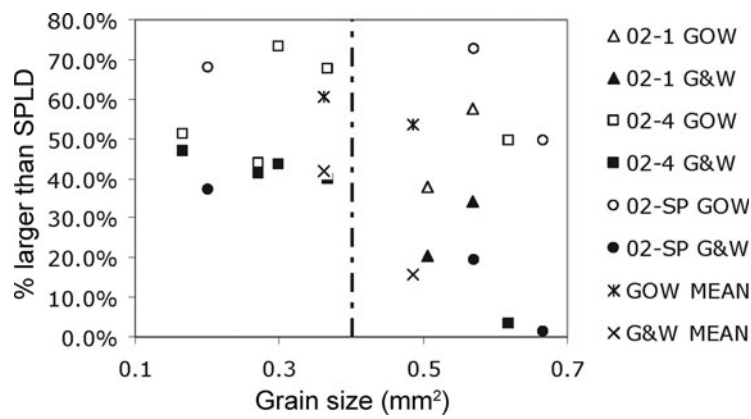
Fig. 5. A potential correlation exists between size/depth and the difference in average grain size between techniques. Mean grain sizes are 60.7% (GOW) and 41.7% (G&W) larger than SPLD when $\overline{G}_{SPLD}$ is <0.4 mm^2, and 53.4% (GOW) and 15.8% (G&W) larger when $\overline{G}_{SPLD}$ >0.4 mm^2.

Comparison of the three techniques applied to samples from the 02-1, 02-4 and 02-SP cores revealed average grain sizes from SEM ($\overline{G}_{SPLD}$) to be significantly smaller than $\overline{G}_{GOW}$ and $\overline{G}_{G\&W}$. $\overline{G}_{GOW}$ are 38–73% larger (average difference ($\overline{D}$) ~57%) using

$$1 - \left(\frac{\overline{G}_{SPLD}}{\overline{G}_{GOW}}\right)$$

compared to $\overline{G}_{SPLD}$, whereas $\overline{G}_{G\&W}$ were only 1–47% larger ($\overline{D} \sim 29\%$) (Fig. 5; Table 1). There are several possible explanations for these differences. The most obvious explanation for the smaller $\overline{G}$ found using SPLD versus GOW is that Gow (1969) uses only the 50 largest grains. This also explains why the difference between $\overline{G}_{SPLD}$ and $\overline{G}_{GOW}$ compared to $\overline{G}_{SPLD}$ and $\overline{G}_{G\&W}$ is greater. There are also several less obvious reasons for the differences. First, traditional methods of grain-size measurement rely on birefringence patterns to distinguish individual grains. Adjacent grains with the same *c*-axis orientations will appear as one, which partially explains the larger $\overline{G}$ found for the GOW and G&W samples. In addition, automated image analysis routines often fail to identify individual grains in firn. Thus grains need to be identified manually, a process which is time-consuming and prone to operator error. These limitations are particularly true for shallow samples where the number of grains in a single thin section is very large. Additionally, the grain boundaries are often blurred and distorted due to the use of pore fillers.

A potential correlation exists between $\overline{G}$ and/or depth and measurement technique. The reduction in grain size derived from SPLD is greatest in small grains. A cut-off grain size of 0.4 mm^2 (approximately the mean of all samples) was used to illustrate this point. $\overline{G}_{GOW}$ is 60.7% larger than $\overline{G}_{SPLD}$, and $\overline{G}_{G\&W}$ is 41.7% larger than $\overline{G}_{SPLD}$ when $\overline{G}_{SPLD}$ is <0.4 mm^2. When $\overline{G}_{SPLD}$ is >0.4 mm^2, the differences decrease to 53.4% (GOW) and 15.8% (G&W). Figure 5 shows the percent difference between $\overline{G}_{SPLD}$ and both $\overline{G}_{GOW}$ and $\overline{G}_{G\&W}$ plotted as a function of depth. Samples with $\overline{G}_{SPLD} < 0.4$ mm^2 have a median depth of 29.45 m; samples with $\overline{G}_{SPLD} > 0.4$ mm^2 have a median depth of 60.16 m. While $\overline{G}_{SPLD}$ of both the shallow and deeper samples are

Table 1. Sample depths, ages, and average grain sizes calculated using the imaging technique of Baker and others (2007) in combination with the measurement technique presented here (SPLD), and the methods of Gow (1969) (GOW) and Gay and Weiss (1999) (G&W). The former uses SEM images of firn samples from the same depths (no pore filler required). The latter two methods utilize crossed-polarized photographs of thin sections prepared using pore fillers (e.g aniline or dodecane).

Sample	Depth	Age	*n*	*G*	Σ	Poss. error
	m	years		mm^2	mm^2	%
SPLD						
02-1-16	16.335	47	60	0.507	0.206	10.85
02-1-32	32.339	98	88	0.569	0.278	13.47
02-4-12	12.918	37	80	0.166	0.084	11.26
02-4-18	17.938	58	45	0.272	0.125	14.07
02-4-42	42.878	152	66	0.3	0.182	14.82
02-4-46	46.853	168	51	0.367	0.191	14.61
02-4-60	60.16	230	59	0.619	0.306	12.88
02-SP-30	29.45	192	77	0.202	0.104	11.65
02-SP-95	94.18	853	63	0.667	0.327	12.34
02-SP-110	109.04	1025	55	0.571	0.328	15.53
GOW						
02-1-16	16.335	47	50	0.815	0.472	6.40
02-1-32	32.339	98	50	1.3408	0.661	7.40
02-4-12	12.918	37	50	0.3413	0.167	6.62
02-4-18	17.938	58	50	0.4837	0.219	5.82
02-4-42	42.878	152	50	1.1204	0.387	5.86
02-4-46	46.853	168	50	1.13	0.149	7.49
02-4-60	60.16	230	50	1.2265	0.560	7.57
02-SP-30	29.45	192	50	0.6277	0.212	4.29
02-SP-95	94.18	853	50	1.3239	0.538	6.72
02-SP-110	109.04	1025	50	2.09	0.603	9.68
G&W						
02-1-16	16.335	47	516	0.637	0.225	7.74
02-1-32	32.339	98	410	0.865	0.342	6.99
02-4-12	12.918	37	250	0.313	0.069	5.72
02-4-18	17.938	58	255	0.462	0.093	5.42
02-4-42	42.878	152	598	0.53	0.193	4.88
02-4-46	46.853	168	598	0.61	0.576	3.71
02-4-60	60.16	230	511	0.641	0.223	5.02
02-SP-30	29.45	192	913	0.321	0.151	6.72
02-SP-95	94.18	853	540	0.676	0.289	6.33
02-SP-110	109.04	1025	489	0.71	0.838	8.19

Table 2. Calculation of repeatability standard deviation (Currie, 1995). The area of 10% of the grains in 19 samples, representing the highest- and lowest-quality cores, was outlined twice with more than a week in between to determine the repeatability of measurements. A correction factor (C_N) to account for the underestimation of the population standard deviation resulting from a sample size of $n = 2$ is applied (Gurland and Tripathi, 1971)

Sample	Trial 1 mm^2	Trial 2 mm^2	σ_r mm^2	$\sigma_r C_N$ mm^2
062-10	0.320	0.328	0.006	0.007
062-20	0.421	0.401	0.014	0.018
062-26	0.367	0.375	0.006	0.007
062-36	0.600	0.555	0.032	0.040
062-50	0.459	0.447	0.008	0.010
062-62	0.510	0.531	0.015	0.019
062-77	0.628	0.580	0.034	0.043
062-83	0.616	0.615	0.001	0.001
062-96	1.036	0.810	0.160	0.200
074-10	0.204	0.173	0.021	0.027
074-19	0.245	0.246	0.001	0.001
074-29	0.231	0.220	0.008	0.010
074-40	0.272	0.274	0.001	0.002
074-50	0.562	0.575	0.010	0.012
074-71	0.231	0.216	0.010	0.013
074-82	0.283	0.262	0.014	0.018
074-90	0.551	0.468	0.059	0.073
074-103	0.657	0.571	0.061	0.076
074-110	0.339	0.349	0.007	0.009
Average				**0.031**

smaller than $\overline{G}_{GOW}$ and $\overline{G}_{G\&W}$, the difference is greatest in the shallower samples. The reduction in grain size obtained from the SPLD technique is greater in small grains and at shallow depths for the following reasons: (1) Previous methods overestimated the size of small grains by including pore filler in the grain outline. The number and size of pores decrease with increasing depth, so this overestimation decreases with depth. (2) Features identified as individual grains in shallow thin sections were probably aggregates of several grains. As grains grow larger, the birefringence within an individual grain becomes more defined, so individual grains are more easily identified. (3) The boundaries of small, shallow grains are better defined in SEM images and consequently identified with greater accuracy.

There is a 25.9% decrease in the difference between $\overline{G}_{SPLD}$ and $\overline{G}_{G\&W}$ for grains smaller than 0.4 mm^2 and those greater than this size. For $\overline{G}_{SPLD}$ versus $\overline{G}_{GOW}$, the decrease is only 7.3% (Fig. 5). A paired t test was performed to determine if the sample means above and below 0.4 mm^2 were significantly different (i.e. if the difference between techniques is really biased towards small grains). $\overline{D}_{\overline{G}_{G\&W}} < 0.4$ mm^2 is not significantly different from $\overline{D}_{\overline{G}_{G\&W}} > 0.4$ mm^2 (one-tail $p = 0.24$). Conversely, $\overline{D}_{\overline{G}_{G\&W}} < 0.4$ mm^2 is significantly different from $\overline{D}_{\overline{G}_{G\&W}} > 0.4$ mm^2 (one-tail $p = 0.009$). The significance and magnitude of the size bias is likely greater in G&W than in GOW because Gay and Weiss (1999) designed their automated outlining program for use on ice, not firn. As discussed above, the use of pore fillers is more problematic in firn than in less porous ice. Thus, as the samples used in this study approach the microstructure of ice, the results derived

using the techniques of Gay and Weiss (1999) become more consistent with those obtained using the SPLD technique. In addition, the variation in small to medium-sized grains is ignored because $\overline{G}_{GOW}$ is calculated using only the 50 largest grains. Because these grains are the most difficult to measure with earlier techniques and are identified with greater accuracy using the new technique, the difference in grain size with depth between $\overline{G}_{GOW}$ and $\overline{G}_{SPLD}$ is expected to be dampened. If all grains were included, the size bias with depth would likely be statistically significant, as it is for $\overline{G}_{G\&W}$.

Sources of measurement error

The estimation of grain size has several sources of potential error including the cut effect, the intersection probability effect and sample processing, as well as inconsistency in the analyst's technique (repeatability), chamber sublimation and population size. The repeatability of SEM grain-size measurements was estimated using 19 samples. One area was randomly selected from an original image where the area of a number of grains equal to approximately 10% of the entire sample total ($n = 4$–25 grains) was determined by creating a new skeleton outline. The area of the newly outlined grains was compared to the area of the grains originally outlined to derive a repeatability standard deviation (σ_r) (Currie, 1995). Variance is a biased estimator of σ when the sample population (n) is small (Montgomery and Runger, 2003), so σ_r was multiplied by a correction factor (C_N) to remove the underestimation. Since measurements were repeated twice, $n = 2$ and C_N is 1.2533 (Gurland and Tripathi, 1971). This procedure was repeated for all depths in the cores with the highest- and lowest-quality samples. The repeatability standard deviations for all samples were averaged to produce the single value. The decision to conduct only two trials on a large number of samples, rather than many trials on a smaller number of samples, was based on the heterogeneous quality of the samples. If many trials were performed on a single high-quality sample, σ_r would be underestimated. Thus, many samples of varying quality were measured twice. σ_r was found to be ± 0.038 mm^2 for the lowest-quality core and ± 0.024 mm^2 for the highest-quality core. These values were averaged to obtain a σ_r value of ± 0.031 mm^2, with $\overline{G}_{MAX} = 1.036$ mm^2, $\overline{G}_{MIN} = 0.173$ mm^2 and $\overline{G}_{MEAN} = 0.435$ mm^2 (Table 2). Thus the standard deviation is ~7% of the mean for the trials and the mean of all the samples in this study ($\overline{G}_{MEAN} = 0.424$ mm^2). The measurements from the two repeatability trials had a correlation coefficient of 0.975. Manually tracing the grain boundaries produces the primary source of error in the repeatability calculation, so it can be assumed that a similar amount of error will be introduced during manual corrections of outlines obtained using the Gay and Weiss (1999) technique. If the SPLD grains are 7% larger than calculated and the G&W grains are 7% smaller, there will still be a 30% difference in grain size between the two techniques for grain sizes smaller than 0.4 mm^2. For grains larger than 0.4 mm^2, measurements from SPLD and G&W may be identical. This is attributed to the increased accuracy of the SPLD technique compared to previous techniques in the measurement of small grains.

Sublimation is known to occur in the SEM chamber (Cullen and Baker, 2001) and is a potential source of uncertainty in grain-size measurements using SEM. If sublimation is too rapid, measured grain areas will increase or

decrease during the experiment depending on where they have been sectioned (i.e. the cut effect). In order to assess repeatability, images taken at the same coordinates were compared at the beginning and end of a session. Approximately 3.5–4 hours elapsed between repeat imaging. During this time, the sample was maintained in the chamber at $-110 \pm 5°C$. The average change in grain size over the 4 hour period was $\pm 0.022\,mm^2$, corresponding to approximately 5% of the mean grain size for all samples in the repeatability test, as well as the mean grain size for all three cores in this study. The change in area during 3.5–4 hours of sublimation is smaller than the repeatability standard deviation. Assuming a constant sublimation rate (Andreas, 2007), there is only a $\pm 0.006\,mm^2$ or a 1.4% change in $\overline{G}_{MEAN}$ during the course of normal imaging (~1–1.5 hours). This value is significantly less than the measure of repeatability (7%). Our analysis shows that chamber sublimation does not cause a statistically significant change in grain size during the course of normal imaging.

The effect of sample size on the reliability of SEM grain-size measurements was also considered. The cold stage used to analyze firn and ice in the SEM restricts the size of the sample to a maximum dimension of 3 cm × 1 cm × 1 cm. As a result, a statistically significant population of certain grain sizes might be difficult to obtain when using only a single sample. The possible error associated with the sample size was calculated for each type of measurement (Table 1) using:

$$\text{possible error} = \frac{t\sigma}{\sqrt{n}},$$

where n is the number of grains analyzed, σ is the standard deviation and t is the one-tailed t statistic at 95% confidence. The average possible error for SPLD is approximately twice that of both GOW and G&W. The inclusion of a larger number of grains (which was not done here) will increase the accuracy.

In a study of grain-size measurements of metals and ceramics using image analysis, Diógenes and others (2005) report a difference of <2% between $\overline{G}$ calculated using approximately 1000 grains versus only 100 grains. While the averages were very similar, the standard deviations were quite different. Standard deviations associated with 100 grain-size measurements were almost 2.5 times greater (40.3% of $\overline{G}$) than those associated with 1000 grain-size measurements (16.5% of $\overline{G}$). Thus it can be assumed that average grain measurements derived from samples with few grains are indicative of the true mean, although the grain-size distribution may be inaccurate. Our sample sizes were too small to obtain 100 grains per sample, but this factor is not critical because our focus is quantifying $\overline{G}$ rather than grain-size distribution.

Growth rate

The transformation of snow to firn to ice results from increasing overburden pressure which causes a decrease in pore spacing. Angular snow grains are initially rounded through contact with one another, which reduces pore space and increases density as the material becomes firn. Porosity is further reduced by sintering, the process through which material is transferred from one grain to another at initial points of contact. These points of contact become grain boundaries. Grain boundaries are interfacial defects in the lattice of any material where there are atomic mismatches in
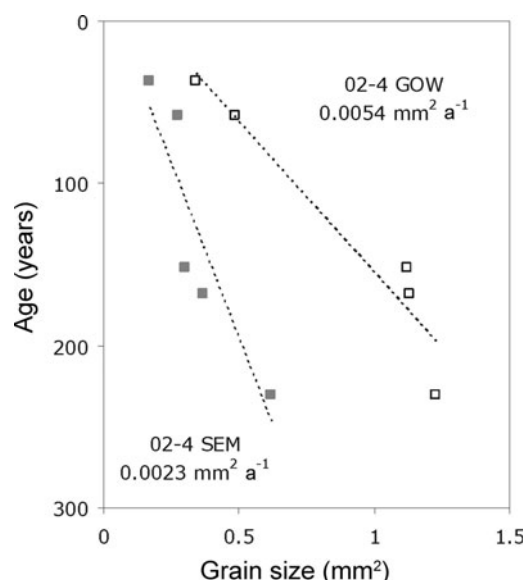

Fig. 6. Determination of growth rate for 02-4 from grain sizes calculated using the technique of GOW (which along with Stephenson (1967) was originally used to define the Arrhenius-type dependence) and SPLD. Data from Table 1.

the transition from the crystalline orientation of one grain to the next (Callister, 2007). In the transformation between firn and ice, there is a steady increase in grain size with depth; this normal grain growth results from a minimization of grain boundary area. Grain boundary migration is driven by the curvature of high-energy grain boundaries and the stored energy difference between grains (Burke, 1949). Small grains are typically found on the concave side of the boundary, and the pressure is typically greatest at this location. Atomic diffusion is in the direction of the low-pressure location, and boundary motion is in the opposite direction. Thus the grain on the high-pressure side becomes incorporated into the grain on the low-pressure side (Callister, 2007; Sieg, 2008), and large grains grow at the expense of smaller grains. The diffusion of molecules occurs over time and is a temperature-dependent process, so growth rates are dependent upon depth (age) and temperature (Paterson, 1994).

For core 02-4, $\overline{G}_{SPLD}$ was found to increase from $0.166\,mm^2$ at 12.9 m (37 years) to $0.619\,mm^2$ at 60.2 m (230 years). Figure 6 shows grain size plotted against age. A linear least-squares best fit of these data gives a rate of increase (growth rate, K) of $0.0023\,mm^2\,a^{-1}$. The same samples yield $\overline{G}_{GOW} = 0.341\,mm^2$ at 12.9 m, $1.226\,mm^2$ at 60.2 m and $K = 0.0054\,mm^2\,a^{-1}$ (Fig. 6), an increase of $0.0031\,mm^2\,a^{-1}$. The values for G&W are $\overline{G}_{G\&W} = 0.313\,mm^2$ at 12.9 m and $0.641\,mm^2$ at 60.2 m and $K = 0.0017\,mm^2\,a^{-1}$, a decrease of $0.0006\,mm^2\,a^{-1}$ compared with K_{SPLD}.

For core 02-SP, $\overline{G}_{SPLD}$ increased from $0.202\,mm^2$ at 29.45 m (192 years) to $0.571\,mm^2$ at 109.04 m (1025 years), with $K = 0.0006\,mm^2\,a^{-1}$. The same samples yield $\overline{G}_{GOW} = 0.628\,mm^2$ at 29.45 m, and $2.090\,mm^2$ at 109.04 m, with $K = 0.0017\,mm^2\,a^{-1}$, an increase of $0.0011\,mm^2\,a^{-1}$. The values for G&W are $\overline{G}_{G\&W} = 0.321\,mm^2$ at 29.45 m, $0.710\,mm^2$ at 109.04 m and $K = 0.0005\,mm^2\,a^{-1}$, a decrease of $0.0001\,mm^2\,a^{-1}$ compared with K_{SPLD}.

The ratio of K_{SPLD} to K_{GOW} is 0.426 for 02-4 and 0.353 for 02-SP. The ratio of K_{SPLD} to $K_{G\&W}$ is 1.353 for 02-4 and 1.2 for 02-SP. It is important to note that K from 02-SP is based
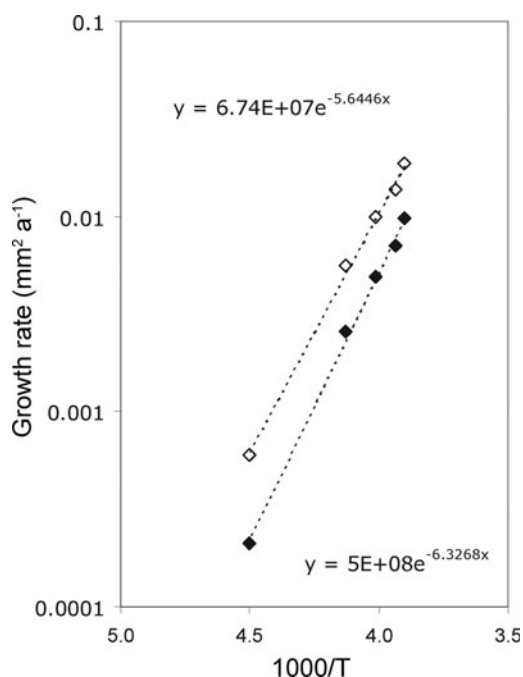
Fig. 7. Grain growth rate versus reciprocal temperature calculated for five sites published by Gow (1969). Open diamonds are original data from Gow (1969). Closed diamonds show the data corrected using the calculated decrease in the ratio of K_{GOW} versus K_{SPLD} per °C increase from –51.0°C of 0.0052°C^{-1}. Activation energies of grain boundary diffusion of 49.6 and 52.6 kJ mol^{-1} are calculated from the slope.

on three points, with no data between 25.5 m (192 years) and 94.1 m (853 years). The purpose of these calculations is to understand the effect of measurement technique on the slope of the *T*–*K* curve. Since the Arrhenius-type dependence of this relationship was originally defined using the techniques of Gow (1969), only SPLD and GOW measurements are used in the calculation of activation energy; data from G&W are not considered.

Activation energy

Activation energy (E_a) is calculated using the equation:

$$E_a = -R\left(\frac{\partial \ln K}{\partial (1/T)}\right),$$

where *R* is the gas constant and the remainder of the term is the slope of the *T*–*K* curve. Because grain size is dependent upon temperature, the size-biased reduction of $\overline{G}_{SPLD}$ versus $\overline{G}_{GOW}$ will affect the magnitude of the calculated activation energy. The validity of the SPLD method can therefore be tested using the previously defined Arrhenius-type temperature dependence of grain growth (Stephenson, 1967; Gow, 1969). To be considered valid, the SPLD method must yield an E_a value consistent with the requisite ~6:10 ratio, as discussed above.

To calculate a new activation energy, growth rates based on grain-size calculations using the SPLD method and encompassing a range of temperature regimes are required. The samples used in this study do not meet the temperature range requirements, so new growth rates were calculated for sites previously evaluated (South Pole, Southice, Maudheim, Wilkes, and Site 2, Greenland; Fig. 1) by Gow (1969). Gow's original growth rates include a single data point from

Greenland. The inclusion of this point is justified because the only variable in question is temperature. Growth rates were calculated using a correction factor based on comparison of *K* values from the SPLD method to those of GOW. The value of the correction factor was determined by dividing the difference between the ratios of $K_{SPLD}:K_{GOW}$ at sites 02-SP and 02-4 (–0.073) by the difference in mean annual temperature between the two sites (–14.0°C) (10 m temperature map provided/compiled by D.A. Dixon; see J. Bohlander and T. Scambos, http://nsidc.org/data/docs/agdc/thermap/documentation.html). The correction factor, 0.0052°C^{-1}, expresses the increase in the ratio of $K_{SPLD}:K_{GOW}$ with each 1.0°C increase in temperature from site 02-SP. Site 02-SP was chosen as the baseline temperature because the South Polar region has near to the lowest mean annual surface temperature on the Antarctic continent.

The correction factor was applied to the sites from Gow (1969) using the equation:

$$K_{SPLDX} = K_{GOWX}[0.353 - 0.0052(T_{02SP} - T_X)]$$

where X is location, 0.353 is the ratio $K_{SPLD}:K_{GOW}$ at 02-SP and *T* is temperature (°C).

The use of this correction factor required the singular assumption that the reduction in growth rate as a function of differences in grain-size measurement technique is nearly identical at sites 02-SP and South Pole. This was considered a valid assumption because both sites have similar mean annual surface temperature and growth rate.

The new growth rates, which changed the slope of the *T*–*K* curve from Gow's (1969) value of –5.6446 K to –6.3268 K, are shown in Figure 7. The apparent activation energy subsequently changed from 46.9 kJ mol^{-1} to 52.6 kJ mol^{-1} (Fig. 7). Nasello and others (2005) and Barr and Milkovich (2008) reported activation energies of grain boundary diffusion of 49 and 51.1 kJ mol^{-1} respectively, values similar to that from SEM analyses. This indicates that, despite the substantial decrease in SEM-derived estimates of $\overline{G}$ and *K* versus those from techniques using photographs of thin sections, the resultant increase in activation energy obtained from the SPLD method still favors the assumption of an Arrhenius-type dependence. However, the increase in calculated activation energy does suggest that the influence of temperature on grain growth is greater than previously indicated, as larger activation energy values indicate that more energy is required to initiate grain boundary migration.

CONCLUSION

Firn grain sizes obtained using SEM images are substantially smaller than those obtained from earlier techniques, on average 57.1% smaller than those calculated using the methods of Gow (1969) and 28.7% smaller than Gay and Weiss (1999). The SPLD technique uses clearly etched grain boundaries and the presence of open pores to identify and measure individual grains from SEM images. This approach allows for a more accurate determination of grain size, porosity and other properties, such as those necessary to characterize firn densification (i.e. surface specific area and contact area; Arnaud and others, 1998), without the need to disrupt the firn microstructure with toxic pore fillers and additional processing, as was the case with earlier methods. New grain growth rates were calculated for older core sites by applying a correction factor equivalent to the ratio of grain sizes obtained from the new technique to those from

previous methods. Newly calculated grain growth rates yield an E_a of grain boundary diffusion of $52.6 \, \text{kJ} \, \text{mol}^{-1}$, similar to those from previous studies. Thus, despite the decrease in grain size, the basic relationship between grain size, growth rate and temperature remains nearly constant. This constancy serves as a validation of the measurement technique.

The new technique presented here streamlines the collection and intercomparison of firn- and ice-core microstructural data. By defining grains as single units in which visibly etched boundaries typically align with a change in axis orientation, a minimum acceptable misorientation between grains can be reported, leading to a more reliable comparison of data. This technique is especially useful for the measurement of very small grains, which are most difficult, if not impossible, to measure using previous techniques. In addition, SEMs typically have associated equipment capable of determining the chemical composition of impurities within the firn and ice, so spatial and temporal variations in the microstructure and chemistry with depth can also be obtained. The capability to identify anomalous stratigraphic layers, study firn densification and metamorphism and co-register physical and chemical microstructural data will enhance the climatic interpretations of ice-core proxies.

REFERENCES

Alley, R.B. 1980. Densification and recrystallization of firn at Dome C, East Antarctica. *Inst. Polar Stud. Rep.* 77.

Alley, R.B. and G.A. Woods. 1996. Impurity influence on normal grain growth in the GISP2 ice core, Greenland. *J. Glaciol.,* **42**(141), 255–260.

Anderson, M.P., G.S. Grest and D.J. Srolovitz. 1989. Computer simulation of normal grain growth in three dimensions. *Philos. Mag. B,* **59**(3), 293–329.

Andreas, E.L. 2007. New estimates for the sublimation rate for ice on the Moon. *Icarus,* **186**(1), 24–30.

Arnaud, L., V. Lipenkov, J.M. Barnola, M. Gay and P. Duval. 1998. Modelling of the densification of polar firn: characterization of the snow–firn transition. *Ann. Glaciol.,* **26**, 39–44.

Baker, I., D. Iliescu, R. Obbard, H. Chang, B. Bostick and C.P. Daghlian. 2005. Microstructural characterization of ice cores. *Ann. Glaciol.,* **42**, 441–444.

Baker, I., R. Obbard, D. Iliescu and D. Meese. 2007. Microstructural characterization of firn. *Hydrol. Process.,* **21**(12), 1624–1629.

Barr, A.C. and S.M. Milkovich. 2008. Ice grain size and the rheology of the Martian polar deposits. *Icarus,* **194**(2), 513–518.

Burke, J.E. 1949. Some factors affecting the rate of grain growth in metals. *Trans. AIME,* **180**, 73–91.

Callister, W.D., Jr. 2007. *Materials science and engineering: an introduction. Seventh edition.* New York, Wiley.

Cole, D.G., P. Feltham and E. Gillam. 1954. On the mechanism of grain growth in metals with special reference to steel. *Proc. R. Soc. London, Ser. B,* **67**(2), 131–137.

Cullen, D. and I. Baker. 2001. Observation of impurities in ice. *Microsc. Res. Tech.,* **55**(3), 198–207.

Currie, L.A. 1995. Nomenclature in evaluation of analytical methods including detection and quantification capabilities (IUPAC Recommendations 1995). *Pure Appl. Chem.,* **67**(10), 1699–1723.

Diógenes, A.N., E.A. Huff and C.P. Fernandes. 2005. Grain size measurement by image analysis: an application in the ceramic and in the metallic inductries. *Proceedings of COBEM 2005. 18th International Congress of Mechanical Engineering, 6-11 November 2005, Ouro Preto, Brazil.* São Paulo, COBEM

Duval, P. and C. Lorius. 1980. Crystal size and climatic record down to the last ice age from Antarctic ice. *Earth Planet. Sci. Lett.,* **48**(1), 59–64.

Gay, M. and J. Weiss. 1999. Automatic reconstruction of polycrystalline ice microstructure from image analysis: application to the EPICA ice core at Dome Concordia, Antarctica. *J. Glaciol.,* **45**(151), 547–554.

Gow, A.J. 1969. On the rates of growth of grains and crystals in South Polar firn. *J. Glaciol.,* **8**(53), 241–252.

Gow, A.J., D. Meese and R. Bialas. 2004. Accumulation variability, density profiles and crystal growth trends in ITASE firn and ice cores from West Antarctica. *Ann. Glaciol.,* **39**, 101–109.

Gurland, J. and R.C. Tripathi. 1971. A simple approximation for unbiased estimation of standard deviation. *Am. Stat.,* **25**(4), 30–32.

Higgins, M.D. 2000. Measurement of crystal size distributions. *Am. Mineral.,* **85**(9), 1105–1116.

Legrand, M. and P. Mayewski. 1997. Glaciochemistry of polar ice cores: a review. *Rev. Geophys.,* **35**(3), 219–243.

Mayewski, P.A. and I. Goodwin. 1997. *US ITASE: science and implementation plan.* (Joint PAGES/GLOCHANT Report.) Bern, PAGES International Project Office.

Mayewski, P.A. *and 18 others.* 2005. The International Trans-Antarctic Scientific Expedition (ITASE): an overview. *Ann. Glaciol.,* **41**, 180–185.

Montgomery, D.C. and G.C. Runger. 2003. *Applied statistics and probability for engineers. Third edition.* New York, Wiley.

Nasello, O.B., C.L. Di Prinzio and P.G. Guzmán. 2005. Temperature dependence of 'pure' ice grain boundary mobility. *Acta Mater.,* **53**(18), 4863–4869.

Obbard, R., I. Baker and K. Sieg. 2006. Using electron backscatter diffraction patterns to examine recrystallization in polar ice sheets. *J. Glaciol.,* **52**(179), 546–557.

Paterson, W.S.B. 1994. *The physics of glaciers. Third edition.* Oxford, etc., Elsevier.

Rick, U.K. and M.R. Albert. 2004. Microstructure and permeability in the near-surface firn near a potential US deep-drilling site in West Antarctica. *Ann. Glaciol.,* **39**, 62–66.

Sieg, K.E. 2008. Examination of the fine-grained region of the Siple Dome ice core. (MS thesis, Dartmouth College.)

Stephenson, P.J. 1967. Some considerations of snow metamorphism in the Antarctic ice sheet in the light of ice crystal studies. *In* Oura, H., *ed. Physics of snow and ice.* Sapporo, Hokkaido University. Institute of Low Temperature Science, 725–740.

Surdyk, S. 2002. Low microwave brightness temperatures in central Antarctica: observed features and implications. *Ann. Glaciol.,* **34**, 134–140.

Thorsteinsson, T., J. Kipfstuhl, H. Eicken, S.J. Johnsen and K. Fuhrer. 1995. Crystal size variations in Eemian-age ice from the GRIP ice core, central Greenland. *Earth Planet. Sci. Lett.,* **131**(3–4), 381–394.

Zwally, H.J., P. Gloersen, W.J. Campbell and R.O. Ramseier. 1977. Analysis of Antarctic ice sheet and sea ice by sequential microwave imagery. *Eos,* **58**(8), 812.